(4)

MARYLAND

COLLEGE PARK CAMPUS

THE PROBLEM OF SELECTING THE SHAPE FUNCTIONS FOR A P-TYPE FINITE ELEMENT

I. Babuška
Institute for Physical Science and Technology
University of Maryland
College Park, MD 20742 USA

M. Griebel
Institute of Informatik
Technical University Munich
Arcisstr 21
D-8000 München 2 FRG

J. Pitkäranta
Department of Mathematics
University of Maryland
College Park, MD 20742 USA
and
Institute of Mathematics, Helsinki
University of Technology
SF 02150
Finland

MD88-36-IB-MG-JP
TR88-36
BN-1090

November 1988

INSTITUTE FOR PHYSICAL SCIENCE AND TECHNOLOGY

Encl (1)

SECURITY CLASSIFICATION OF THIS PAGE (When Data Entered)

REPORT DOCUMENTATION PAGE		READ INSTRUCTIONS BEFORE COMPLETING FORM
1. REPORT NUMBER BN-1090	2. GOVT ACCESSION NO.	3. RECIPIENT'S CATALOG NUMBER
4. TITLE (and Subtitle) The Problem of Selecting the Shape Functions for a p-Type Finite Element		5. TYPE OF REPORT & PERIOD COVERED Final life of contract 6. PERFORMING ORG. REPORT NUMBER
7. AUTHOR(s) I. Babuska[1], M. Griebel[2], J. Pitkäranta[3]		8. CONTRACT OR GRANT NUMBER(s) [1]ONR N00014-85-K-0169 [2]ONR N00014-85-K-0169 [2]Tech. Univ. of Munich [3]Finnish Academy/Univ. of MD
9. PERFORMING ORGANIZATION NAME AND ADDRESS Institute for Physical Science and Technology University of Maryland College Park, MD 20742		10. PROGRAM ELEMENT, PROJECT, TASK AREA & WORK UNIT NUMBERS
11. CONTROLLING OFFICE NAME AND ADDRESS Department of Navay Office of Naval Research Arlington, VA 22237		12. REPORT DATE November 1988 13. NUMBER OF PAGES 35
14. MONITORING AGENCY NAME & ADDRESS(if different from Controlling Office)		15. SECURITY CLASS. (of this report) 15a. DECLASSIFICATION/DOWNGRADING SCHEDULE

16. DISTRIBUTION STATEMENT (of this Report)

Approved for public release: distribution unlimited

17. DISTRIBUTION STATEMENT (of the abstract entered in Block 20, if different from Report)

18. SUPPLEMENTARY NOTES

19. KEY WORDS (Continue on reverse side if necessary and identify by block number)

20. ABSTRACT (Continue on reverse side if necessary and identify by block number)

The paper addresses the question of the optimal selection of the shape functions for p-type finite elements and discusses the effectivity of the conjugate gradient and multilevel iteration method for solving the corresponding linear system.

DD FORM 1 JAN 73 1473 EDITION OF 1 NOV 65 IS OBSOLETE

S/N 0102-LF-014-6601

SECURITY CLASSIFICATION OF THIS PAGE (When Data Entered)

THE PROBLEM OF SELECTING THE SHAPE FUNCTIONS FOR A P-TYPE FINITE ELEMENT

I. Babuška
Institute for Physical Science and Technology
University of Maryland
College Park, MD 20742 USA

M. Griebel
Institute of Informatik
Technical University Munich
Arcisstr 21
D-8000 Munchen 2 FRG

J. Pitkäranta
Department of Mathematics
University of Maryland
College Park, MD 20742 USA

and

Institute of Mathematics, Helsinki
University of Technology
SF 02150
Finland

MD88-36-IB-MG-JP

TR88-36

November 1988

[1]Partially supported by the Office of Naval Research under Contract N00014-85-K-0169.

[2]Supported by Technical University Munich and Office of Naval Research under Contract N00014-85-K-0169.

[3]Supported by the Finnish Academy and by the Department of Mathematics, University of Maryland.

Abstract. The paper addresses the question of the optimal selection of the shape functions for p-type finite elements and discusses the effectivity of the conjugate gradient and multilevel iteration method for solving the corresponding linear system.

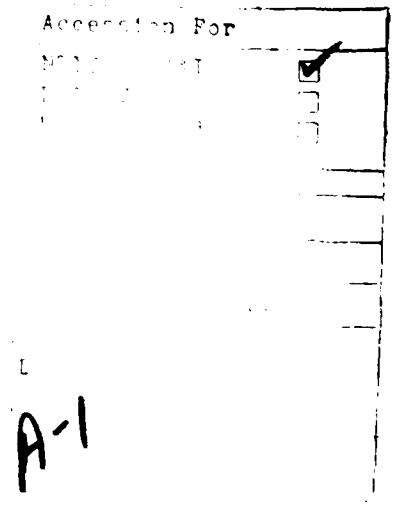

A-1

1. Introduction.

A natural way to treat the finite element method on a parallel computer is to associate to every available processor a superelement. The main computational work is then on the *superelement* level and can be made completely in parallel. The global part of the computation which is not well parallelizable is then a relatively minor part of the entire computation.

The superelement can be for example constructed by the p-version of the finite element method, by the domain decomposition technique where the superelement consists of a grid of finer elements, etc.

The complexity of such a superelement approach (based on the p-version) depending on the computer architecture was studied in [1], [2]. See also [3], [4].

We can understand the superelement as a linear space S of trial function spanned by certain basis (shape) functions. The convergence and accuracy of the finite element method then depend on the approximation properties of S and is of course independent of the particular choice of the basis of S. On the other hand, the computational effectivity of the finite element method depends also for example on the effectivity of an iterative solver, the sensitivity of a direct solver round-off errors, etc., which depends directly on the choice of the basis functions.

The main mathematical tool of analyzing the performance of the numerical method is the asymptotic analysis with respect to some parameters, such as $p \longrightarrow \infty$ in the p-version, or $h \longrightarrow 0$ in the h-version. Such an analysis is effective in practice *only* if the asymptotic range encompasses the practical values of these parameters. Unfortunately, this is not always the case. Let us mention for example the p-version. Here the performance of certain iterative method (see below) can be characterized by a parameter $\mathcal{H}(p)$ which is

known to grow asymptotically as $\mathcal{H}(p) \sim (\lg p)^2$. However, as in practice one mostly has $p \leq 10$, the asymptotic analysis neglecting the precise behavior of $\mathcal{H}(p)$ for small p is not sufficient. Although the asymptotic analysis is still important, practical insight in the performance of a method can be obtained only together with a proper computational analysis. The aim of this paper is to make such a computational analysis and to get an insight into various aspects related to the choice of basis (shape) for p-type finite element functions. We will restrict ourselves here only to the case of a scalar equation in two dimensions and to a quadrilateral element.

A more general and thorough analysis will be given in forthcoming papers.

2. The quadrilateral superelement.

We will discuss the case of a unit-square superelement, which can also be understood as a master element.

Let us consider the unit square Ω (the master element) as shown in Figure 2.1

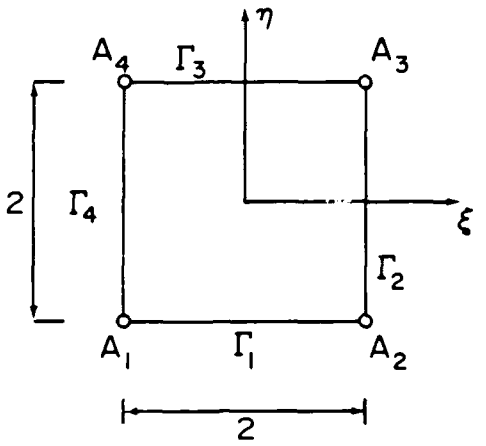

Figure 2.1. The master element

with the vertices A_i and sides Γ_i. Denote by $\{\psi_i\}$ the set of shape functions used in the finite element method. Then these functions are of three groups associated with the vertices, sides and interior of the element. They are called

1) nodal shape functions

2) side shape functions

3) internal shape functions.

1) *The nodal shape function* is associated to a vertex A_i of the element Ω. It is zero on the opposite sides of the vertex it is associated to.

2) *The side shape function* is associated to a side Γ_i and is zero on all three other sides of the element.

3) *The internal shape function* is zero on all four sides, i.e., it has a character of the "bubble" function.

In addition to the above mentioned properties of the shape functions we require typically that the basis is invariant under rotations of the coordinates by $k \times 90^{\circ}$, $k = 1,2,3$. We require, of course, that the span S of the shape function have good approximation properties, too.

The shape functions are not uniquely determined by the above requirements. For example, we can add to any nodal or side shape function an internal shape function and still preserve all the properties mentioned above.

Usually the set of shape functions is a one parameter set (say with the parameter $t = 1,2,\ldots$). In the case of the p-version $t = p$ and in the h-version we take $t = \frac{1}{h}$. We can now impose an additional constraint on the set of shape functions, namely the requirement that the shape function are hierarchic. By this we mean that if $\{\psi^{[t]}\}$ is the basis of $S(t)$ for given t then $\{\psi^{[t+1]}\} \supset \{\psi^{[t]}\}$, i.e., the set $\{\psi^{[t+1]}\}$ of shape functions can be obtained by an augmentation of the set $\{\psi^{[t]}\}$. The property of hierarchicity is desirable if the computation is to be made with many values of the parameter t, such as in adaptive computations.

3. Examples of shape functions.

In this section we will introduce some sets of the shape functions that we will consider in the next sections.

A. The hierarchic set Q'_p of the p-version. This set is for example used in the computer program PROBE.

1) The nodal shape functions. There are the usual bilinear functions:

$$N_1(\xi,\eta) = \frac{1}{4}(1-\xi)(1-\eta)$$

$$N_2(\xi,\eta) = \frac{1}{4}(1+\xi)(1-\eta)$$

$$N_3(\xi,\eta) = \frac{1}{4}(1+\xi)(1+\eta)$$

$$N_4(\xi,\eta) = \frac{1}{4}(1-\xi)(1+\eta)$$

2) The side shape functions. There are (p-1) shape functions associated with every side Γ_i, $\nu = 1,2,3,4$. These are defined as

$$N_i^{[1]}(\xi,\eta) = \frac{1}{2}(1-\eta)\Phi_i(\xi), \quad i = 1,2,\ldots,p-1,$$

$$N_i^{[2]}(\xi,\eta) = \frac{1}{2}(1+\xi)\Phi_i(\eta), \quad i = 1,2,\ldots,p-1,$$

$$N_i^{[3]}(\xi,\eta) = \frac{(-1)^i}{2}(1+\eta)\Phi_i(\xi), \quad i = 1,2,\ldots,p-1,$$

$$N_i^{[4]}(\xi,\eta) = \frac{(-1)^i}{2}(1-\xi)\Phi_i(\xi), \quad i = 1,2,\ldots,p-1,$$

where

$$\Phi_i(\xi) = \sqrt{\frac{2i-1}{2}} \int_{-1}^{\xi} P_i(t)dt$$

and $P_j(t)$ is the Legendre polynomial of degree j. The term $(-1)^i$ is needed in $N_i^{[3]}$ and $N_i^{[4]}$ to obtain invariance with respect to the rotation

of coordinates.

3) The internal shape functions. For $p < 4$ there are no internal shape functions. For $p \geq 4$ there are $(p-2)(p-3)/2$ internal shape functions defined as

$$N^{[0]}_{i,j}(\xi,\eta) = (1-\xi^2)(1-\eta^2)P_i(\xi)P_j(\eta), \quad 0 \leq i+j \leq p-4.$$

For example, if $p = 8$ there are 47 shape functions consisting of 4 nodal, 28 side and 15 internal shape functions.

The set Q'_p is the minimal set which includes all polynomials of degree p and which has the properties listed above. This guarantees the good approximation properties of the span. Let us mention that this set does not include all polynomials of degree p in both variables ξ and η separately. The span is identical with the span of the serendipity elements and is denoted by Q'_p as in [5]. The introduced set of the shape functions is obviously heirarchal one with respect to the parameter p = degree. These shape functions are sufficiently orthogonal in typical applications, so that their use does not lead to large problems with round-off errors in connection with direct solvers.

B. The hierarchal set Q_p of the p-version. This set includes all polynomials of degree p in *each* variable. Hence it differs from the set Q'_p only by using now $(p-1)^2$ internal shape functions. The set Q_p has thus $(p+1)^2$ shape functions in comparison with $\frac{p^2}{2}+\frac{3}{2}p+3$ shape functions in the set Q'_p.

C. The quasiorthogonal set O_p of the p-version. Let $\Phi_i(\xi)$, $i = 1,\ldots,p-1$, be polynomials of degree $\leq p$, such that $\Phi_i(-1) = \Phi_i(1) = 0$, and

$$\int_{-1}^{+1} \Phi_i'(\xi)\Phi_j'(\xi)d\xi = \delta_{ij}, \quad i,j = 1,\ldots,p-1$$

$$\int_{-1}^{+1} \Phi_i(\xi)\Phi_j(\xi)d\xi = 0, \quad i \neq j.$$

This set is uniquely determined as the (finite element) eigenfunctions of the eigenvalue problem: Find the pairs $(\Phi_i,\lambda_i) \in V_p \times \mathbb{R}$, $i = 1,\ldots,p-1$, such that

$$\int_{-1}^{+1} \Phi_i'(\xi)v'(\xi)d\xi = \lambda_i \int_{-1}^{+1} \Phi_i v d\xi \quad \forall\, v \in V_p$$

where

$V_p = \{v | v$ is a polynomial of degree $\leq p$ on $[-1,1]$ and $v(-1) = v(1) = 0\}$.

The eigenvalues λ_i are positive and distinct. Further, let $\varphi_i(\xi)$, $i = 1,\ldots,p-1$, be another set of polynomials of degree $\leq p$ such that $\varphi_i(-1) = 1$, $\varphi_i(1) = 0$ and

$$\int_{-1}^{+1} \varphi_i' v' d\xi + \lambda_i \int_{1}^{1} \varphi_i v d\xi = 0 \quad \forall\, v \in V_p,$$

where λ_i are the eigenvalues mentioned above. The functions φ_i are uniquely determined. To see it we write

$$\varphi_i(\xi) = \chi(\xi) + \varphi_i^*(\xi),$$

$$\chi(\xi) = \frac{1}{2}(1-\xi).$$

Then $\varphi_i^*(\xi) \in V_p$ is the (finite element) solution of the problem

$$\int_{-1}^{+1} \varphi_i^{*\prime} v' d\xi + \lambda_i \int_{1}^{1} \varphi_i v d\xi = -\int_{-1}^{+1} (\chi' v' + \lambda_i \chi v) d\xi, \quad v \in V_p,$$

and since $\lambda_i > 0$ φ_i^* exists and is uniquely determined. Now we define

1) the nodal shape functions. They are the same as in the set Q'_p.

2) The side shape functions. The side shape functions associated with Γ_1 are

$$N_i^{[1]}(\xi, \eta) = \Phi_i(\xi)\varphi_i(\eta), \quad i = 1, 2, \ldots, p-1.$$

The shape functions associated with the sides Γ_j, $j = 2, 3, 4$, are defined analogously. Hence as before we have $(p-1)$ side shape functions associated with every side Γ_j.

3) The internal shape functions. There are $(p-1)^2$ internal shape functions as in the system Q_p. The shape functions associated with Γ_1 are then

$$N_{k,\ell}^{[0]}(\xi, \eta) = \Phi_k(\xi)\Phi_\ell(\eta), \quad k, \ell = 1, \ldots, p-1.$$

This system O_p has all properties as the system Q_p except that the system O_p is not a hierarchal one. On of the hand, it has various useful orthogonality properties which will be mentioned later.

D. <u>The h-version set H_p of the shape functions</u>. Here the span S will be the set if piecewise bilinear functions on the uniform mesh with $h = \frac{2}{p}$. The shape functions are the usual "hat" functions which obviously can be divided into the groups of the nodal side and internal shape functions.

In addition we will consider the set H_p^+ where the nodal shape functions of the set H_p are replaced by those of the set Q'_p.

E. <u>The trigonometric set T_p of the shape functions</u>. For theoretical

reasons we will also consider the set of shape functions where only side shape functions are present and defined by

$$N_i^{[1]}(\xi,\eta) = \cos \frac{i\pi}{2} \xi \sin h \frac{i\pi}{2}(1-\eta), \quad i = 1,2,\ldots,p-1,$$

for side Γ_1 and analogously for the other sides. Note that these functions are harmonic.

4. The optimal selection of the shape functions.

Let the set $\{\psi_i\}$ of the shape functions be given. Then in the finite element method we construct first the local stiffness matrix $A = \{a_{ij}\}$, $a_{ij} = B(\psi_i, \psi_j)$ where $B(u,v)$ is the bilinear form on which the finite element method is based. The global stiffness matrix is constructed by the usual assembly process. In this paper we will restrict our analysis to the case of one superelement only. We will assume that the bilinear form is associated to the Laplace operator, i.e.,

$$B(\psi_i, \psi_j) = \int_\Omega \left[\frac{\partial \psi_i}{\partial \xi} \frac{\partial \psi_j}{\partial \xi} + \frac{\partial \psi_i}{\partial \eta} \frac{\partial \psi_j}{\partial \eta} \right] d\xi d\eta. \tag{4.1}$$

The stiffness matrix A is uniquely (up to permutation) defined by the set of shape functions. We will always assume that the shape functions are rescaled (preconditioned) so that $a_{i,i} = 1$ (i.e., all diagonal terms of A are equal to one). This will sometimes be called trivial preconditioning.

Now we can formulate what we mean by optimal shape function selection according to various criteria.

A. The criterion of the minimal condition number.

We will say that the shape functions are optimal if the condition number of the local stiffness matrix (after trivial preconditioning) is minimal among all choices of the shape functions (with the same span) which preserve the categories of the nodal, side and internal shape functions, the invariances with respect to the rotation defined earlier. We can also impose additional constraints as the hierarchy of of the shape functions.

The motivation of this notion is to get the most effective conjugate gradient method (see section 6) or to maximize the numerical stability of the direct solution method. The exact structure of these optimal shape functions

is not known.

Realizing that the performance of the conjugate gradient method depends not only on the condition number (e.g., on the clustering of the eigenvalues) we have

B. The criterion of the maximal decay number (i.e., reduction of the residuum by one iteration) in the conjugate gradient method.

Here the obvious goal is to achieve the required accuracy with minimal number of iterations.

We can, of course, design other criteria of optimality. In this paper we will mostly address the criterion A. We approach the optimization problem formulated above via numerical experiments so as to obtain the information in the practical range of p, say for $1 \leq p \leq 20$.

5. Computational analysis of the set Q_p'.

We will first analyze the condition number of the (local) stiffness matrix A when using the bilinear form (4.1). Since the first eigenvalue $\lambda_1 = 0$ we define the condition number $\mathcal{H}(A) = \frac{\lambda_{max}}{\lambda_2}$ and call λ_{max} and $\lambda_{min} = \lambda_2$ the dominant eigenvalues. To get a proper insight we will compute the condition number of various combinations of the shape functions. The results are shown in Table 5.1.

Table 5.1.

Condition number $\mathcal{H}$ of various portions of the stiffness matrix of set set Q_p'.

p	Internals + Sides + Nodals	Internals	Sides	Sides + Nodals	Internals + Nodals	Internals + Sides
1	1.50			1.50	1.50	
2	5.78		1.36	5.77	1.50	1.36
3	5.78		2.33	5.77	1.50	2.33
4	22.1	1.00	2.70	5.96	1.50	22.1
5	23.9	1.00	2.84	5.96	1.50	23.6
6	62.8	3.09	2.92	5.96	3.09	62.8
7	67.7	4.53	2.95	5.96	4.53	66.7
8	203.0	12.8	2.97	5.96	12.8	203.0

The first column in Table 5.1 depicts the condition number of the whole stiffness matrix. The condition number $\mathcal{H}(A)$ grows as p^3 (see Figure 5.1). Upon comparing the columns of Table 5.1 we see that the dominating factor in the growth of the condition number is the coupling between the side and

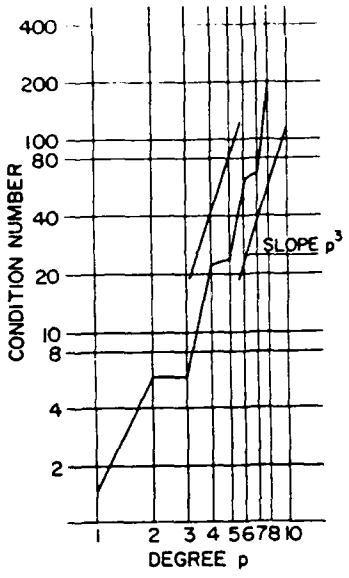

Figure 5.1. The condition number $\mathcal{H}(A)$ for the set Q'_p.

internal shape functions. Other coupling such as sides-sides, sides-nodals, internals-internals, are relatively much weaker except in the low range ($1 \leq p \leq 3$) where there are no internals. We are then led to the conclusion that in seeking for an optimal set of shape functions, the first step should be to reduce this coupling between the side and internal shape functions. Below we will remove the coupling completely by eliminating (condensation) the internals (this can be done in parallel when many superelements are present). Although this very likely does not lead to an exactly optimal basis, we conjecture that we can in this way construct shape functions which are close to the optimal ones (in the sense of criterion A).

The above mentioned elimination can be interpreted as changing the side shape function so that they are "harmonic" in the finite element sense. This removes the coupling between internals and side shape functions but increases the coupling between side shape functions. Of course, the hierarchy of the shape functions is lost. Note that the nodal shape functions are bilinear and

hence harmonic, so they are orthogonal to the internal shape functions.

We will now address this decoupling in more detail. Given p we will order the shape functions so that the internals come first, i.e., we write

$$\Psi = [\Psi^{[1]}, \Psi^{[2]}]^T$$

where

$$\Psi^{[1]} = [\psi_1^{[1]}, \ldots, \psi_N^{[1]}]$$

are the internal shape functions. The stiffness matrix can be written now in a block way

$$A = \begin{bmatrix} A_{11} & A_{12} \\ A_{12}^T & A_{22} \end{bmatrix}.$$

Here the block A_{11} corresponds to the internals. The decoupling is performed by a transformation into the new basis

$$\hat{\Psi} = [\Psi^{[1]}, \Psi^{[2]}]$$

where

$$\hat{\Psi}^{[2]} = M_2[\Psi^{[2]} - A_{12}^T A_{11}^{-1} \Psi^{[1]}]. \tag{5.1}$$

Here M_2 is a diagonal (normalizing) matrix to be defined shortly. In this new set of shape functions the stiffness matrix takes the form

$$\hat{A} = BAB^T = \begin{bmatrix} A_{11} & 0 \\ 0 & M_2 \tilde{A}_{22} M_2^T \end{bmatrix} \tag{5.2}$$

where

$$B = \begin{bmatrix} I_1 & 0 \\ 0 & M_2 \end{bmatrix} \begin{bmatrix} I_1 & 0 \\ -A_{12}^T A_{11}^{-1} & I_2 \end{bmatrix} \tag{5.3}$$

and

$$\tilde{A}_{22} = A_{22} - A_{12}^T A_{11}^{-1} A_{12}. \tag{5.4}$$

By I_1 and I_2 we denote the identity blocks. $\tilde{A}_{22}$ is the Schur complement of A with respect to A_{11}. We finally define the diagonal matrix $M = \begin{bmatrix} I_1 & 0 \\ 0 & M_2 \end{bmatrix}$ so that $[\hat{A}]_{i,i} = 1$ for all i, i.e., we set

$$[M]_{ij} = [\tilde{A}]_{i,i}^{-1/2} \delta_{i,j} \tag{5.5}$$

Since the nodal shape functions are bilinear (and harmonic) there is no coupling between the nodals and interiors. Therefore the transformation (5.1) changes only the side shape functions. The shape functions $\hat{\psi}_i^{[2]}$ are such that

$$B(\hat{\psi}_i^{[2]}, \varphi) = 0$$

for any $\varphi = \psi_i^{[1]}$, i.e., $\hat{\varphi}^{[2]}$ are discretely harmonic.

If $A_{11}^{-1} A_{12}$ in (5.4) is computed using the Cholesky decomposition $A_{11} = LL^T$ then we obtain as a by-product new interior basis functions $\hat{\varphi}^{[1]}$ which are orthogonal, i.e., with $\hat{\psi}_i^{[1]} = L^{-T} \psi_i^{[1]}$ we get

$$B(\hat{\psi}_i^{[1]}, \hat{\psi}_j^{[1]}) = \psi_i^{[1]T} L^{-1} A L^{-T} \psi_i^{[1]} = \delta_{i,j},$$

and hence the stiffness matrix for these new internals is the unit matrix. The system of the shape functions $\hat{\psi} = [\psi^{[1]}, \hat{\psi}^{[2]}]$ constructed above will be denoted by $Q_p'^*$, and the system of shape functions $[\hat{\psi}^{[1]}, \hat{\psi}^{[2]}]$ will be denoted by $\tilde{Q}_p'^*$.

Remark 5.1. Note that $\hat{A}_{22}$ is the stiffness matrix that remains in the finite element system where the degrees of freedom for the internal shape functions are eliminated (condensed out). We will call the element where the

interior degrees of freedom are removed a condensed element. Thus in the condensed element there are no internal shape functions. The side shape functions are "discretely harmonic" with respect to the original internals, and the condensed matrix is the Schur complement of the original stiffness matrix with respect to its interior block.

Let us now consider matrix $\hat{A}$ as defined by (5.2) through (5.5). In Table 5.2 we give the dominant (i.e., the smallest non-zero and the largest eigenvalue of A_{11} and $\hat{A}_{22} = M_2^T \tilde{A}_{22} M_2$) as well as the condition number $\hat{A}$ for $p = 1,\ldots,8$.

Table 5.2.

Dominant eigenvalues of A_{11} and $\hat{A}_{22} = M_2 \tilde{A}_{22} M^T$ and $\mathcal{H}(\hat{A})$ for the shape functions of Q'^{*}_{p}.

p	$\lambda_{min}(A_{11})$	$\lambda_{min}(\hat{A}_{22})$	$\lambda_{max}(A_{11})$	$\lambda_{max}(\hat{A}_{22})$	$\mathcal{H}(\hat{A})$
1		1.0		1.50	1.50
2		0.346		2.00	5.78
3		0.346		2.00	5.78
4	1.0	0.253	1.0	2.20	8.69
5	1.0	0.242	1.0	2.24	9.26
6	0.524	0.190	1.62	2.26	11.9
7	0.402	0.177	1.82	2.26	12.8
8	0.183	0.141	2.35	2.26	16.7

Comparing Tables 5.1 and 5.2 we see that removing the coupling between the internal and the side shape functions reduces the condition number of the stiffness matrix quite dramatically. We see that $\mathcal{H}(\hat{A})$ grows with p much more slowly than $\mathcal{H}(A)$. Note also that since A_{11} has no contribution to $\mathcal{H}(\hat{A})$ in view of Table 5.2, there is no reason for constructing better (e.g.,

orthogonal) internal shape functions $\hat{\psi}^{[1]}$ at least in the range $1 \le p \le 8$. In this range the condition numbers of the set Q'^{*}_{p} and $\tilde{Q}'^{*}_{p}$ are the same and also the condition number of the condensed element is the same as that of $\tilde{Q}'^{*}_{p}$.

So far we have not addressed the shape functions on the sides Γ_i. To assess their influence on the condition number let us construct orthogonal normalized shape functions $\hat{\hat{\psi}}^{[2]}$ and the corresponding stiffness matrix $\hat{\hat{A}}$ namely such that $[\hat{\hat{A}}]_{ij} = 0$ for $i \neq j$ in the following cases:

a) $\hat{\hat{\psi}}^{[2]}_i$ and $\hat{\hat{\psi}}^{[2]}_j$ are both internal shape functions;

b) $\hat{\hat{\psi}}^{[2]}_i$ is an internal shape function and $\hat{\hat{\psi}}^{[2]}_j$ is the side shape function;

c) $\hat{\hat{\psi}}^{[2]}_i$ and $\hat{\hat{\psi}}^{[2]}_j$ are both side shape functions corresponding to the one side.

These shape functions are obviously decoupled in a maximaly orthogonal way under the constraint imposed in section 2, namely preserving the groups of nodal side and internal shape functions.

We can construct the shape functions as follows. Let $\hat{\psi}$ be the shape functions already constructed. Let $\hat{A}_0$ be the matrix (of the same size as the matrix $\hat{A}$) such that

1) $[\hat{A}_0]_{ii} = 1$ for all i;

2) $[\hat{A}_0]_{ij} = [\hat{A}]_{ij}$ for $i \neq j$ in any of the cases a,b,c mentioned above;

3) $[\hat{A}_0]_{ij} = 0$ otherwise.

Let further $\hat{A}_0 = CC^T$ be the Cholesky decomposition of $\hat{A}_0$. Then we define the new shape functions

$$\hat{\hat{\psi}} = C^{-T}\hat{\psi}.$$

The corresponding stiffness matrix is then

$$\hat{\hat{A}} = C^{-1}\hat{A}C^{-T}. \tag{5.6}$$

These shape functions $\hat{\hat{\psi}}$ satisfy all desired properties as well as the stiffness matrix $\hat{\hat{A}}$ (with $[\hat{\hat{A}}]_{i,i} = 1$). This set $\hat{\hat{\psi}}$ of shape functions will be denoted by $Q_p'^{**}$.

Remark 5.2. For symmetry reasons it is obviously sufficient to compute the new shape functions associated to only one side, say Γ_1, and then to use simple transformations to get the side shape functions on the other sides.

Remark 5.3. The above method of constructing maximally orthogonal functions is universal in the sense that it obviously apply to any set of shape functions. For example, we can construct in a similar way the sets Q_p^{**}, H_p^{**} and H_p^{+**}. We can construct the shape functions. There are many other ways of constructing maximally orthogonal systems of shape functions. For example, the set O_p mentioned above is such as is easily checked.

Remark 5.4. The shape functions $\hat{\psi}$ and $\hat{\hat{\psi}}$ are obviously not hierarchic. For computational reasons it may be desirable to keep the new stiffness matrix in the product form (5.2), (5.6), so that the non-hierarchic part (matrices B and C^{-1}) is separated from the hierarchic part (matrix A). In the many-element case (such as on grid of quadrilaterals), it is sufficient to compute B and C^{-1} on a reference element only. This sacrifices in general the orthogonality but essentially preserves the good conditioning if the elements are not too much distorted.

In Table 5.3 below we give the dominant eigenvalues and the condition number $\mathcal{H}(\hat{\hat{A}})$ for $p = 1,\ldots,8$.

Table 5.3.

Dominant eigenvalues and condition number for the shape functions of Q'^{**}_p.

p	$\lambda_{min}(\hat{\hat{A}})$	$\lambda_{max}(\hat{\hat{A}})$	$\mathcal{H}(\hat{A}$
1	1.0	1.50	1.50
2	0.346	2.00	5.78
3	0.346	2.00	5.78
4	0.253	2.20	8.69
5	0.244	2.24	9.19
6	0.200	2.26	11.3
7	0.187	2.27	12.1
8	0.157	2.28	14.5

Comparing Tables 5.2 and 5.3 we see that the orthogonalization of the side shape functions (i.e., the maximal orthogonalization) does reduce the condition number but the effect is not large in the range $1 \leq p \leq 8$, (at most 13%).

6. Comparison of various sets of shape functions.

We will compare in this section the condition numbers of the stiffness matrices for the sets of shape functions which were introduced in the previous sections. Based on the analysis we made in section 5 for the system Q'_p we restrict ourselves only to the case of condensed elements (see Remark 5.1). As we have seen, this restriction is equivalent to the case where the sets $\tilde{Q}'^{*}_p$, $\tilde{Q}^{*}_p$, $\tilde{H}^{*}_p$, etc., instead of Q'_p, Q_p, H_p, etc., are used. The shape function of the set T_p are harmonic functions. Hence we consider them as condensed shape functions (i.e., $T_p = \tilde{T}^{*}_p$).

In Table 6.1 we present condition numbers of the condensed stiffness matrices for various sets of shape functions for $p = 4n + 1$, $n = 1,\ldots,5$ (as before, the shape functions are normalized so that the stiffness matrix has ones on the diagonal).

Table 6.1.

Condition number of the stiffness matrix for $p = 4n + 1$, $n = 1,\ldots,5$ for various sets of shape functions.

	1	2	3	4	5	6	7
p	$\tilde{Q}'^{*}_p$	Q'^{**}_p	$\tilde{Q}^{*}_p$	O_p	$\tilde{H}^{*}_p$	$\tilde{H}^{+**}_p$	$\tilde{T}^{*}_p$
5	9.3	9.2	15.5	14.2	5.4	14.7	11.4
9	16.3	14.8	28.0	22.4	10.2	20.2	15.8
13	23.4	19.5	39.8	28.5	14.9	45.2	18.7
17	30.7	23.8	51.3	33.5	19.7	62.3	20.9
21	37.8	27.4	62.5	37.8	24.4	80.4	22.7

We see that the condition number of the condensed stiffness matrix grows relatively slowly with p in all cases except for $\tilde{H}^{+*}$. It can be theoretically shown that in the cases O_p, Q^{**}_p and $\tilde{T}_p$ the growth is asymptotically at worst of order $O((\log p)^2)$, i.e., there is a constant independent of p

such that

$$\mathcal{H}(p) \le C[(\log p)^2]. \tag{6.1}$$

We refer to [6], [7] for relevant results. Figure 6.1 shows the condition number $\mathcal{H}(p)$ in the $1\times(\log p)^2$ scale (in the range $5 \le p \le 21$) for all considered cases. For example, in the case of the set Q_p, $\mathcal{H}(p)$ can be expressed rather accurately by

$$\mathcal{H}(p) \approx 5.6 + 3.5(\log p)^2 \tag{6.1a}$$

in the range $9 \le p \le 21$, or by

$$\mathcal{H}(p) \approx 2.3 + 2.6 \log p + 3.0(\log p)^2 \tag{6.1b}$$

in the whole range $5 \le p \le 21$.

In the cases $\tilde{Q}_p'^{*}$, $\tilde{Q}_p^{*}$, $\tilde{H}_p^{+*}$ the growth of the condition number is expected to be larger due to the nonorthogonality of the side shpae functions. This nonorthogonality is largest in the case $\tilde{H}_p^{+*}$. Here one can show that the growth role is asymptotically at least $\mathcal{H}(p) \sim p$ and at worst $\mathcal{H}(p) \sim p(\log p)^2$. The impact of these nonorthogonalities is clearly visible in Figure 6.1.

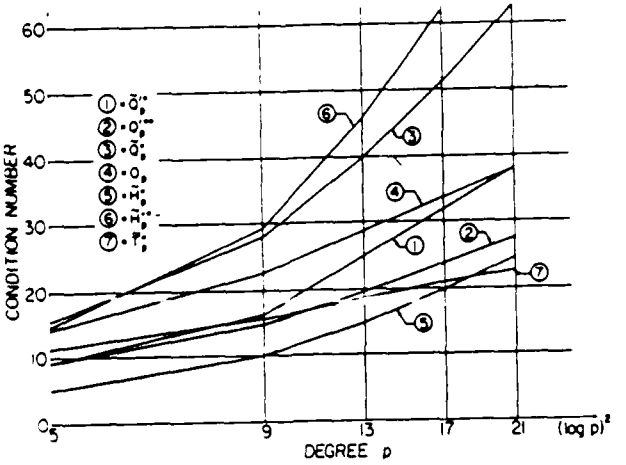

Figure 6.1.

Condition number $\mathcal{H}(p)$ for various sets of shape functions

1) = $\tilde{Q}_p'^{*}$, 2) = $Q_p'^{**}$, 3) = $\tilde{Q}_p^{*}$, 4) = Q_p^{**}, 5) = $\tilde{H}_p^{*}$, 6) = $\tilde{H}_p^{+*}$, 7) = $\tilde{T}_p^{*}$

Let us finally point out that in the practical range of p (see Table 6.1 and Figure 6.1) the element of the type Q'_p seems superior to Q_p-type element (with the same value of p) even if the side shape functions of Q are orthogonalized (i.e., when the set O_p is considered) and those of Q'_p are not (i.e., when we use the set $\tilde{Q}'^{*}_p$). In the orthogonalized cases the condition numbers of the set Q'^{**} are about 30% less than of the set O_p. It also seems from Figure 6.1 that the growth of $\mathcal{H}(p)$ for the set Q'^{**}_p and O_p is the same (i.e., $\mathcal{H}(p) \approx O(\log p)^2$) but this has not been proven theoretically yet.

Remark 6.1. It seems that generally the condition number of the condensed polynomials is better when less internal shape functions are present in the original set. For example, let us modify the set Q_p so that it includes the internals of the set Q_q (this set will be denoted by $Q_{p,q}$).

Table 6.2 shows the condition number of the reduced stiffness matrix corresponding to two adjacent sides and the node inbetween for $p = 11$ and varying q. We see that the condition number grows monotonically with q. This indicates that the coupling between the sides becomes stronger as q grows.

Table 6.2.

Condition number of the set $\tilde{Q}^{*}_{11,q}$ reduced to two adjacent sides and the node in between.

q	2	3	4	5	6	7	8
H(q)	3.59	5.82	8.01	10.1	12.2	14.2	16.2

q	9	10	11	12	13	14	15
H(q)	18.2	20.2	22.1	23.0	23.7	23.9	24.1

The results shown in Table 6.2 are in constrast with the theory behind the estimate (6.1) which is proven only if $q \geq p$, see [7].

Remark 6.2. So far we have assumed in all cases that the nodal shape functions are bilinear. The practical reasoning behind this is that the span of these shape functions contains the constant function, which makes it possible to use the nodal block of the stiffness matrix as an effective precondition for the iterative method in the many-element case. For more see [6], [7].

It is of interest to see how the couplings between the nodal and side functions affects the conditioning of the condensed stiffness matrix. In Tables 6.3a,b we give some results indicating the strength of this coupling. In Table 6.3a we show the condition number of the set $\tilde{Q}_p'^*$ and of the same set when the nodals are removed from the original set (this set will be denoted by $\tilde{Q}_{p,0}'^*$). In Table 6.3b we show the condition number of $\tilde{Q}_p^*$ and the same set when the nodal are condensed out (eliminated). This set will be denoted by $\tilde{Q}_{p,00}^*$.

The columns 5 and 6 in Table 6.1 indicate how the condition number in the h-version is affected when the nodal shape functions are changed from the usual "hat" function to the bilinear one.

Table 6.3a.

The condition number of the sets $\tilde{Q}'^{*}_{p}$ and $Q'^{*}_{p,0}$.

p	$\tilde{Q}'^{*}_{p}$	$Q'^{*}_{p,0}$
2	5.78	1.36
3	5.78	2.33
4	8.69	6.00
5	9.26	6.00
6	11.9	8.32
7	12.8	8.13
8	16.1	11.2

Table 6.3b.

The condition number of the sets $\tilde{Q}^{*}_{p}$ and $\tilde{Q}^{*}_{p,00}$.

p	$\tilde{Q}^{*}_{p}$	$Q^{*}_{p,00}$
2	8.69	6.0
3	8.78	6.0
4	15.5	10.9
5	15.5	10.9
6	22.0	15.3
7	22.0	15.3
8	28.0	19.6
9	28.0	19.6
10	34.0	23.8
11	34.0	23.8

We see that in the practical range of p the coupling between the nodal and the side shape functions may affect the condition number by a factor 1.5 to 3. The effect is strongest in the case of the h-version.

We underline that in practice when multi-element approach is used, we do preconditioning by $p = 1$, i.e., we are condensing out the nodal shape

functions and hence the second columns in Tables 6.3b essentially governs the effectivity of the conjugate gradient method.

Let us summarize the main conclusions we have seen so far.

a) The main source of the large condition number of the stiffness matrix of the p-type element with hierarchic shape functions (sets Q'_p, Q_p) is the strong coupling between the side and internal shape functions. This coupling can be removed only by introducing a non-hierarchic set of shape functions.

b) The orthogonalization of the side shape functions (for the sets Q'^{*}_p and Q^{*}_p) improves the condition number, the more the higher the value of p. In the range $1 \leq p \leq 10$ the effect of orthogonalization is at most 40%.

c) The nodal functions contribute to the condition number by about 30%. It is advantageous to remove them in the preconditioning phase.

d) The condition number of the condensed matrix improves in the practical range of p if there are less internal shape functions. Hence the set Q'_p is preferable over the set Q_p.

e) The condensed h-type superelement (set H^{*}_h) behaves in a very similar way as the Q_p-element.

f) The condition number of the condensed Q_p- or H_p-type element grows approximately linearly with $(\log p)^2$ as $p \longrightarrow \infty$ provided that the side shape functions are orthogonal. In the range $1 \leq p \leq 20$, deviations from this theoretical growth are minor for all considered sets.

7. Iterative methods.

In this section we will consider some aspects of the selection of shape functions on the performance of two basic iterative methods, the conjugate gradient method and the multi-level method.

A. The conjugate gradient method. We consider the case of only one element of type $\tilde{Q}'^{*}_{p}$ or $\tilde{Q}^{*}_{p}$ with nonorthogonal shape functions. The multi-element conjugate gradient method is analyzed in [2], [7], where also various aspects of parallel implementation are addressed. Table 7.1 shows the average convergence role (the decay factor) of 10 iterations using the condensed matrix when random initial solution was used. More precisely, Table 7.1 reports ρ_{10} = {energy norm of the error after 10 steps/energy norm of the initial error}$^{1/10}$.

Table 7.1.

The average convergence rate of the conjugate gradient method for the condensed sets $\tilde{Q}'^{*}_{p}$ and Q^{*}_{p}.

p	$\rho_{10}(Q'_p)$	$\rho_{10}(Q_p)$
4	.251	.380
5	.328	.400
6	.398	.503
7	.465	.468
8	.419	.577
9	.450	.492
10	.442	.580
11	.470	.525

The non-monotone behavior of $\rho_{10}(\tilde{Q}'^{*}_{p})$ and $\rho_{p}(Q^{*}_{p})$ shown in the Table is due to random choice of the initial error. We see that the set $\tilde{Q}'^{*}_{p}$ performs better thatn $\tilde{Q}_{p}$ as expected from the previous study of the condition

number study in the previous section. Note that for $p \leq 3$ the conjugate gradient method converges in less than ten steps in both cases.

In Table 7.2 we compare the average convergence rate after ten iterations to the theoretical worst-case rate, see [8],

$$\bar{\rho}_n = \left\{ \frac{2}{\left(\frac{\sqrt{\mathcal{H}}+1}{\sqrt{\mathcal{H}}-1}\right)^n + \left(\frac{\sqrt{\mathcal{H}}-1}{\sqrt{\mathcal{H}}+1}\right)^n} \right\}^{1/n}$$

where $\mathcal{H}$ is the condition number of the stiffness matrix.

Table 7.2.

The actual average convergence rate and the theoretical (worst) rate after 10 iterations for the condensed set Q'_p and Q_p.

p	$\rho_{10}(\tilde{Q}'^{*}_p)$	$\bar{\rho}_{10}(\tilde{Q}'^{*}_p)$	$\rho_{10}(\tilde{Q}^{*}_p)$	$\bar{\rho}_{10}(\tilde{Q}^{*}_p)$
6	.398	.590	.503	.695
11	.470	.679	.525	.758

We see that the conjugate gradient method converges significantly faster than it would be in the theoretical worst case. It is likely related to the clustering of the eigenvalues of the matrix. In Figure 7.1a, respectively 7.1b, we have depicted the density (histogram) of the eigenvalues of the condensed element of the set $\tilde{Q}^{*}_p$, respectively the set Q_p for $p = 21$. We see that the spectrum is sparse at its ends, most of the eigenvalues being clustered around the point $\lambda = 1.0$. (For example, 56 of the 83 are non-zero eigen-eigenvalues of the system Q_{21} are located on the interval [0.9, 1.1].) The clustering is more pronounced in the case Q_p (where the side shape functions are orthogonalized) in comparison with the case of the set $\tilde{Q}^{*}_p$. Apparently, this explains why the actual rate of convergence reported in Tables 7.1 and 7.2 is better than that for the worst possible spectrum.

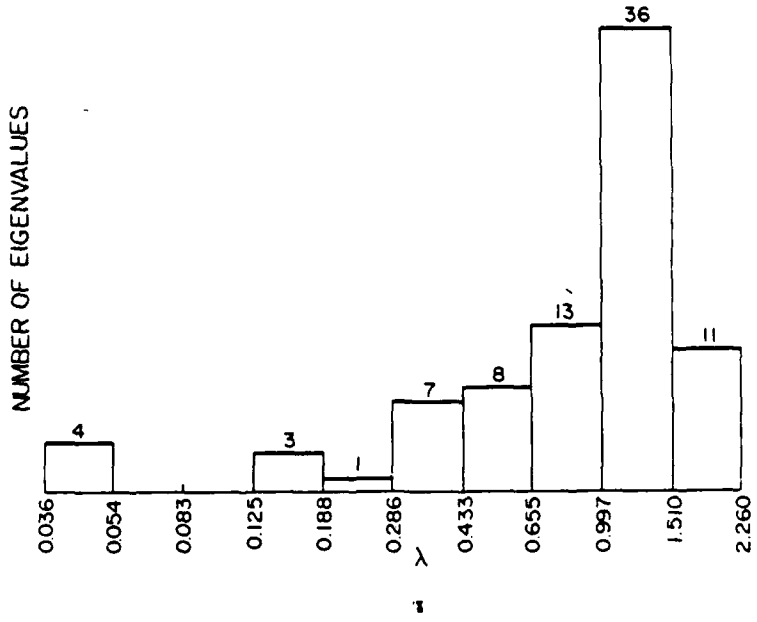

Figure 7.1a

The density of the eigenvalues of the set $\tilde{Q}_p^*$.

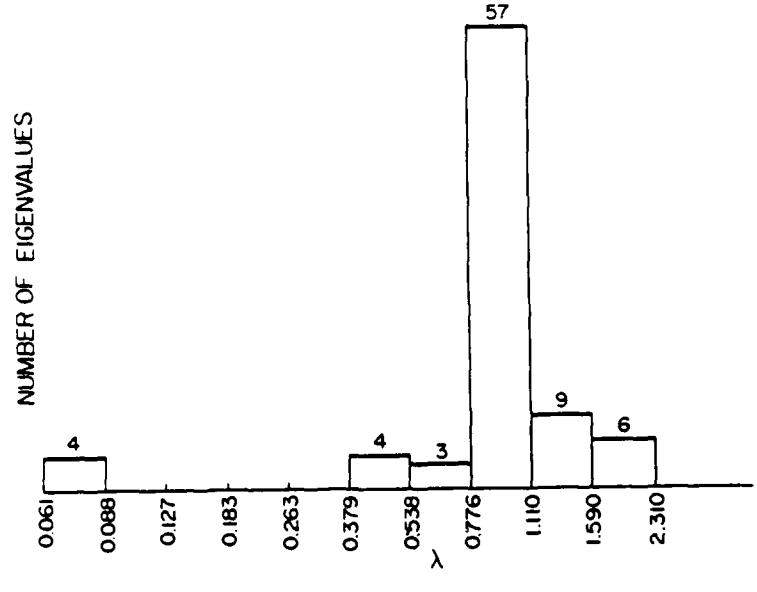

Figure 7.1b

The density of the eigenvalues of the set O_p.

Let us finally mention that the above qualitative nature of the spectrum, i.e., the clustering around the point $\lambda = 1$ with sparse spectrum elsewhere is characteristic to all elements (i.e., sets of shape functions) we considered. The clustering gets relatively stronger when p grows or when the side shape functions are orthogonalized.

B. Multi-p iterations. The multigrid method is widely used in connection with the finite difference method (see e.g. [9]). The same formal idea can be used for the p-method when exploiting the hierarchic character of the bases functions, see also [3].

We will now address the multi-p iterative procedures also in combination with inner type iterations. We will address only the bases functions of the set Q'_p which were introduced in section 3. Mostly we will consider only the case $p = 8$; the cases $p < 8$ will be mentioned only briefly. First, let us introduce some basic notions.

1) The hierarchies. Let us describe the hierarchies we will later use. The hierarchy consists of the sequence $\{p_i\}$ of levels (degrees) which will be iterated one at a time in the sequel.

$$H_1 = \{87654321\}$$

$$H_2 = \{8421\}$$

$$H_3 = \{8642\}$$

$$H_4 = \{87531\}.$$

By iteration on the level p_i, we mean iteration of all shape functions of degree $\leq p_i$ while the shape functions fo degree $p > p_i$ are kept "frozen."

2) As in the classical multigrid we have to deal with cycles. We will use three different cycles.

\CYCL(H_1): It consists of repetition of the hierarchies. For example,

$\backslash CYCL(H_1)$ = {876543218765...2187...}.

$/CYCL(\mathcal{H}_1)$: It consists of the repetition of the hierarchies in the opposite order. For example $/CYCL(H_2)$ = {1248,1248,...}.

$\backslash/CYCL(H_1)$: It consists in the repetition of the hierarchies in the combination form \and/. For example, $\backslash/CYCL(H_3)$ = {8642468642...}.

On every level p we will perform s "inner" SOR(ω) iterations with the overrelaxation parameter ω. Obviously $\omega = 1$ coincides with the Gauss-Seidel iteration. The ordering is as mentioned in section 3.

Table 7.3 shows the asymptotic convergence rate ρ in the H^1-norm (i.e., the decay of the error measured in the H^1-norm when performing one entire iteration cycle) for $p = 8$, $s = 5$, $\omega = 1.8$ and $\omega = 1$.

Table 7.3

The rate of convergence ρ for
various cycles and hierarchies ($p = 8$, $s = 5$).

	\CYCLE $\omega = 1.8$	/CYCLE $\omega = 1.8$	\/CYCLE $\omega = 1.8$	\CYCLE $\omega = 1.0$
H_1	0.425	0.537	0.323	0.686
H_2	0.514	0.507	0.535	0.820
H_3	0.463	0.363	0.497	0.731
H_4	0.445	0.355	0.449	0.731

The value $\omega = 1.8$ is close to the optimal for $p = 8$ and all hierarchies. As an illustration we show in Table 7.4 the dependence of ρ on ω, for $\backslash CYCL(\mathcal{H}_1)$ and $s = 5$.

Table 7.4.

The rate of convergence ρ for $\backslash CYCL(H_1)$, $s = 5$, $p = 8$.

ω	ρ	ω	ρ
0	1.0	1.6	0.446
0.2	0.947	1.7	0.428
0.4	0.891	1.8	0.425
0.6	0.829	1.825	0.426
0.8	0.761	1.85	0.435
1.0	0.686	1.875	0.505
1.2	0.603	1.9	0.583
1.4	0.516	2.0	1.00

Table 7.4 has shown the performances of various cycles for $\omega = 1.0$ and 1.8 and for $p = 8$. The results for $p < 8$ are analogous. As a typical case, we show the convergence rate for $\backslash CYCL(H_1)$ with $s = 5$, $\omega = 1.8$ and $\omega = 1.0$.

Table 7.5.

The rate of convergence ρ for $\backslash CYCL(H_1)$ with $s = 5$, $\omega = 1$, 1.8

p	4	5	6	7	8
$\omega = 1$	0.380	0.411	0.499	0.516	0.686
$\omega = 1.8$	0.325	0.323	0.369	0.331	0.425

So far we presented the results only for $s = 5$. In Table 7.6 we show the dependence of the rate ρ on s in the case $\backslash CYCL(H_1)$ for $p = 8$ and $\omega = 1.8$.

Table 7.6.

The rate of convergence ρ for $\backslash CYCLE(H_1)$, $\omega = 1.8$, $p = 8$.

s	1	2	3	4	5
ρ	0.890	0.748	0.514	0.508	0.426
s	6	7	8	9	10
ρ	0.379	0.298	0.258	0.220	0.196

Above we have shown the rate ρ for the multi-p iteration. In Table 7.7 we show the rate ρ for the SOR iteration for $p = 8$.

Table 7.7.

The convergence rate ρ for SOR(ω), $\omega = 1.0$, 1.8 and $p = 8$.

	SOR(1.0)	SOR(1.8)
ρ	0.966	0.943

From Tables 7.6 and 7.7 we easily conclude that the multi-p iteration is more effective (smaller number of operations) than the SOR iteration for $p = 8$. The overrelaxation clearly improves the performance. The $\backslash CYCL(H_1)$ is most effective. Nevertheless we conclude that the multi-p approach is less effective than in the classical multigrid method for the finite different equations, at least in the form as we have used. The section of the shape functions could obviously also be geared to the optimal performance of the multi-p method, but the problem seems wide open.

We further conclude that this conjugate gradient method applied to the *condensed* elements is clearly superior.

Let us now briefly compare the two iterative methods we have addressed. The conjugate gradient method is very effective when using the condensed ele-

ments and possibly orthogonalized shape functions. The error decays (in the energy norm) by one iteration by a factor 2 or more (for Q'_p element with $p < 11$).

The multi-p method with the hierarchic Q'_p shape functions does not use the condensation which was based on the elimination procedure which is relatively expensive especially for high p. On the other hand, it leads to the need of more iterations when counting the inner iterations of the entire cycle. The combined overrelaxation scheme behaves similarly. Nevertheless, counting all operations of a cycles in comparison with the direct Gauss-Seidel or overrelaxation the multi-p performance is somewhat better.

The conjugate gradient method is very good if condensation is made. Without condensation the rate is not good (e.g., for $p = 8$ we get $\bar{\rho} = 0.93$). Among the schemes studied we recommend the conjugate gradient method with condensation and with preconditioning with $p = 1$ in the multielement case.

8. Conclusions.

The selection of the shape functions is of major importance for the performance of the solver based on iterative methods. Neither the theory nor practice of the optimal selection of the shape functions is available yet.

We have seen that the condensation approach which has obvious advantages from the point of parallel computations is a very effective tool for keeping the condition number under the control and is especially advantageous for the conjugate gradient method. The set Q'_p of the shape functions performs better than Q_p in the practical range of p. Although we addressed only the case of one element only a very similar situation occurs for the mesh of elements where $p = 1$ preconditioning is made. For the analysis of the performance of the conjugate gradient method on complex meshes we refer to [2] where the parallel computation aspects are especially addressed.

For the theoretical analysis we refer to [7].

We discussed only quadrilateral elements. We expect that the triangular elements will lead to a similar performance, but extensive tests are not available yet.

Finally we would like to underline that we addressed only two-dimensional cases. One cannot extrapolate from these results the behavior of three-dimensional elements.

References

[1] Babuška, I., Elman, H.C., Some Aspects of Parallel Implementation of the Finite Element Method on Message Passing Architectures, Univ. of Maryland, Computer Science Tech. Report., UMIACS-TR-88-35, CS-TR-2030.

[2] Babuška, I., Elman, H.C., Markley, K., Parallem Implementation of the Conjugate Gradient for the p-Version of Finite Elements, to appear.

[3] Foresti, S., Brusimo, G., Sonnad, V., Multilevel Solution Method for the p-Version of Finite Elements, Parallel Implementation and Comparison with other Solution Methods, IBM Kingston Tech. Report KGN-137 (1988).

[4] Herbin, R., Gerbi, S., Sonnad, V., Parallel Implementation of a Multigrid Method on the Experimental LCAP Supercomputer II, IBM Kingston Tech. Report KGN-155 (1987).

[5] Ciarlet, P.G., The Finite Element Method for Elliptic Problems, North Holland, Amsterdam, 1978.

[6] Bramble, J.H., Pasciak, J.E., Schatz, A.H., Construction of Preconditions for Elliptic Problems by Substructurings IV, Report BNL-40820 (1988), Brookhaven Nat. Lab.

[7] Babuška, I., Craig, A., Mandel, J., Pitkäranta, J., The Conjugate Gradient Method for the p-Version of the Finite Element Method, to appear.

[8] Axelsson, O., Solution of Linear Systems of Equations: Iterative Methods, in Sparse Matrix Techniques, Lecture Notes in Math. No. 572 (1977), pp. 2-49.

[9] Haskbusch, W., Multigrid Methods and Applications, Springer, New York (1981).

The Laboratory for Numerical analysis is an integral part of the Institute for Physical Science and Technology of the University of Maryland, under the general administration of the Director, Institute for Physical Science and Technology. It has the following goals:

- To conduct research in the mathematical theory and computational implementation of numerical analysis and related topics, with emphasis on the numerical treatment of linear and nonlinear differential equations and problems in linear and nonlinear algebra.

- To help bridge gaps between computational directions in engineering, physics, etc., and those in the mathematical community.

- To provide a limited consulting service in all areas of numerical mathematics to the University as a whole, and also to government agencies and industries in the State of Maryland and the Washington Metropolitan area.

- To assist with the education of numerical analysts, especially at the postdoctoral level, in conjunction with the Interdisciplinary Applied Mathematics Program and the programs of the Mathematics and Computer Science Departments. This includes active collaboration with government agencies such as the National Bureau of Standards.

- To be an international center of study and research for foreign students in numerical mathematics who are supported by foreign governments or exchange agencies (Fulbright, etc.)

Further information may be obtained from Professor I. Babuška, Chairman, Laboratory for Numerical Analysis, Institute for Physical Science and Technology, University of Maryland, College Park, Maryland 20742.